Journal of Sound and Vibration (1998) **218**(3), 501–525
Article No. sv981837

FAULT DETECTION AND MONITORING OF A BALL BEARING BENCHTEST AND A PRODUCTION MACHINE VIA AUTOREGRESSIVE SPECTRUM ANALYSIS

J. P. Dron

Groupe de Mécanique Appliquée, *IUT Léonard de Vinci*, *rue des Crayéres*, *B.P.* 1035, 51687 *Reims Cedex* 2, *France*

AND

L. Rasolofondraibe and C. Couet

Laboratoires d'Applications de la Micro-électronique, *IUT Léonard de Vinci*, *rue des Crayéres*, *B.P.* 1035, 51687 *Reims Cedex* 2, *France*

AND

A. Pavan

Groupe de Mécanique Appliquée, *IUT Léonard de Vinci*, *rue des Crayéres*, *B.P.* 1035, 51687 *Reims Cedex* 2, *France*

(*Received* 26 *September* 1997, *and in final form* 30 *June* 1998)

This paper deals with the implementation of parametric spectrum analysis using the high-resolution technique in setting up conditional maintenance via vibration analysis on a forming press. To achieve this, the resolution power of signal-modelling-based parametric techniques is shown through spectrum assessment computation. The processing of the experimental results enabled (i) various AR spectrum analysis methods and especially Burg's algorithm to be tested, and (ii) conventional spectrum analysis techniques such as the correlogram to be compared with parametric methods at a detection level as well as for mechanical component fault monitoring, especially ball bearing defects. Among various possible models, the AR model was retained along with Burg's algorithm and the AIC criterion. A detection and spotting methodology of faults likely to occur on rotating machinery was developed on the basis of the results which were obtained. This methodology, supplementing other analysis techniques, relies on the understanding of component spectrum behaviour and various constraints to be mastered such as component access availability and problems due to industrial measuring device spectrum resolution, as well as static properties of the power spectrum density assessors of a random signal. The results show that parametric methods are particularly worthwhile in the early detection of component defects, especially when two typical frequencies are close to one another. However, the complexity of these techniques necessitates many precautions when they are implemented; consequently, they should not replace conventional methods, but supplement them.

0022–460X/98/480501 + 25 $30.00/0

1. INTRODUCTION

To be competitive one has, among other things, to maintain manufacturing tools in perfect working order so as to reduce maintenance and repair delays as much as possible. To reach this goal, various maintenance policies may be considered, but the most rational is to implement a conditional maintenance policy. This is based on analysis techniques and process monitoring and must be efficient and easy to implement. Among the different methods in use, the machine vibration and monitoring technique is presently the most widespread. This consists of monitoring on a time scale the evolution of the vibratory signal of a mechanical system to assess the mechanism damage.

There exist several methods to characterize and to monitor the condition of every essential rotating machinery component (see, e.g., reference [1]). Each of these techniques copes with various phenomenon understanding levels and the use of more or less developed analysis devices. Among the vibration signal analyses and kinds of processing available, the AR spectrum analysis has certainly been one of the most important and widespread in industry since spectrum analyzers made their appearance. However, the resulting spectrum is too rich in sinusoidal components blurred with parasitic noises, which often makes it difficult to exploit the obtained spectra. Moreover, most industrial measuring devices have limited signal acquisition characteristics (predefined frequency range, limited sample number, . . .). Thus, to tell apart some very close typical frequencies becomes difficult. Therefore, more efficient analysis techniques able to distinguish very close sinusoidals independently of the resolution power of the measuring device are required.

In this paper, an experimental procedure dealing with fault monitoring and particularly those resulting from quasi-identical components giving very close typical frequencies is provided. This procedure is based on the use of an autoregressive spectrum analysis along with Burg's algorithm and the AIC criterion. Various constraints such as vibration variations, sensor position, measuring parameters like frequency range and sample number were taken into account in order to determine the choice of the suitable technique(s) depending on these parameters.

An industrial implementation of sensitive forming press component damage monitoring, which relies on a judicious choice of vibration monitoring conditions and on the use of the retained so-called "high-resolution" analysis technique which supplements conventional analyses, is presented (time analysis: RMS value, kurtosis; frequency analysis: envelop and spectrum analyses).

2. THE IMPLEMENTED SIGNAL ANALYSIS METHODS

Research has been done to highlight and monitor the mechanical component damaging condition of rotating machinery. When a complex or protected (forming press) machine is involved in the process it is often difficult to position the sensor near every component to be monitored. Therefore, several components are

monitored from the same sensor position. The acquired signal does display the whole mechanical component vibration signature. The use of more efficient techniques is required to enable more efficient diagnosis [2].

2.1. CONVENTIONAL TECHNIQUES

Along with the traditional AR parametric spectrum analysis method, a conventional spectrum assessment technique was implemented (i.e., the correlogram). It was then possible to compare these techniques and to highlight the contribution of the former at the early stage of fault detection and the monitoring of the components sensitive to rotating machinery. The conventional method is based on Fourier's transform of the vibration autocorrelation function in association with a Hanning-type weighting window (correlogram): i.e.,

$$S_x(f) = r(0) + 2\sum_{p=1}^{N-1} r(p)\cos(2\pi pf), \tag{1}$$

where $r(p)$ denotes the assessment of autocorrelation coefficients.

2.2. THE AR SPECTRUM ANALYSIS METHOD

Parametric spectrum analysis methods were defined and developed in signal processing in the spectrum analysis domain in order to determine signal power spectrum density. This enabled signal characteristics to be obtained beyond the conventional methods bound resolution based on Fourier's transform [3]. These methods, known as high resolution techniques, have numerous application domain, recently in the vibration analysis of rotating machinery [4].

Parametric spectrum analysis methods rely on time-modelling the signal. This modelling consists of the assumption that the observed signal is generated by the action of a linear filter on a white noise. The spectral analysis problem then reduces to the identification of the filter model where the number of parameters is obtained by minimizing the error between the measured signal and the output of the model according to an optimality criterion [5]. The power spectrum density is then computed from the recorded model.

The class of parametric methods which provides the model of a random process with an ARMA (Autoregressive Moving Average), AR (Autoregressive), or MA (Moving Average) type model is among the most conventional and above all the most widely used in vibration analysis [6].

The major problems encountered when implementing parametric spectrum analysis methods lie in the choice of (i) the vibration signal representation model, and (ii) the model parameter computing algorithm, and (iii) the model order selection criterion, i.e., the number of its parameters since it is a polynomial model.

Among signal representation models, the AR model was chosen here since it is the best compromise between temporal representation and speed, efficiency and simplicity of algorithms enabling the computation of model parameters. The AR model is currently being used for the detection of the most common mechanical defects via the parametric spectrum analysis. Besides spotting typical frequencies of rotating machinery sensitive components, AR modelling allows the detection

of the presence of vibration signal local non-stationarities through the error of linear prediction. These non-stationarities display, in most cases, component defects, such as on a gearing system [7].

The AR model is provided with the recurring equation

$$e(n) = y(n) + \sum_{i=1}^{p} a_i y(n-i). \tag{2}$$

Here $e(n)$ represents the linear or residual prediction error, a_i represents the model parameters, and $y(n)$ represents the sensor output value.

The a_i parameter value is obtained via the solution of a linear system, the so-called Yule–Walker equations, which depict the relationship between model parameters and signal correlation coefficients (or correlation matrix/array). Yule–Walker equations can be obtained either with the maximal entropy condition or via a linear prediction method. Burg's algorithm enables one, however, to assess model parameters directly from the observed data without having recourse to the intermediary step of correlation matrix assessment. Burg's algorithm is based on the arithmetic mean of direct and regressive prediction error powers. The direct prediction error is defined by

$$e_m^f(n) = x(n) + \sum_{i=1}^{m} a_{m,i} x(n-i). \tag{3}$$

The regressive prediction error is provided by

$$e_m^b(n) = x(n-m) + \sum_{i=1}^{m} a_{m,i} x(n+i-m). \tag{4}$$

By introducing Levinson's recurring principle in the definition, error recurring relations are obtained:

$$e_m^f(n) = e_{m-1}^f(n) + K_m e_{m-1}^b(n-1), \qquad e_m^b(n) = e_{m-1}^b(n-1) + K_m e_{m-1}^f(n). \tag{5, 6}$$

Burg's criterion is the arithmetic mean of direct and regressive prediction error powers:

$$C_m = \frac{1}{2(N-p+1)} \left[\sum_{n=m}^{N} (|e_m^f(n)|^2 + |e_m^b(n)|^2) \right]. \tag{7}$$

By replacing $e_m^f(n)$ and $e_m^b(n)$ with relations (5) and (6), e_m becomes a single K_m parameter function, for at m order prediction errors at $m-1$ are known. Resetting the C_m derivation with respect to K_m provides the K_m assessment:

$$K_m = -\frac{2 \sum_{n=m}^{N} e_{m-1}^f(n) e_{m-1}^b(n-1)}{\sum_{n=m}^{N} (|e_{m-1}^f(n)|^2 + |e_{m-1}^b(n-1)|^2)}. \tag{8}$$

Therefore, the algorithm is as follows:

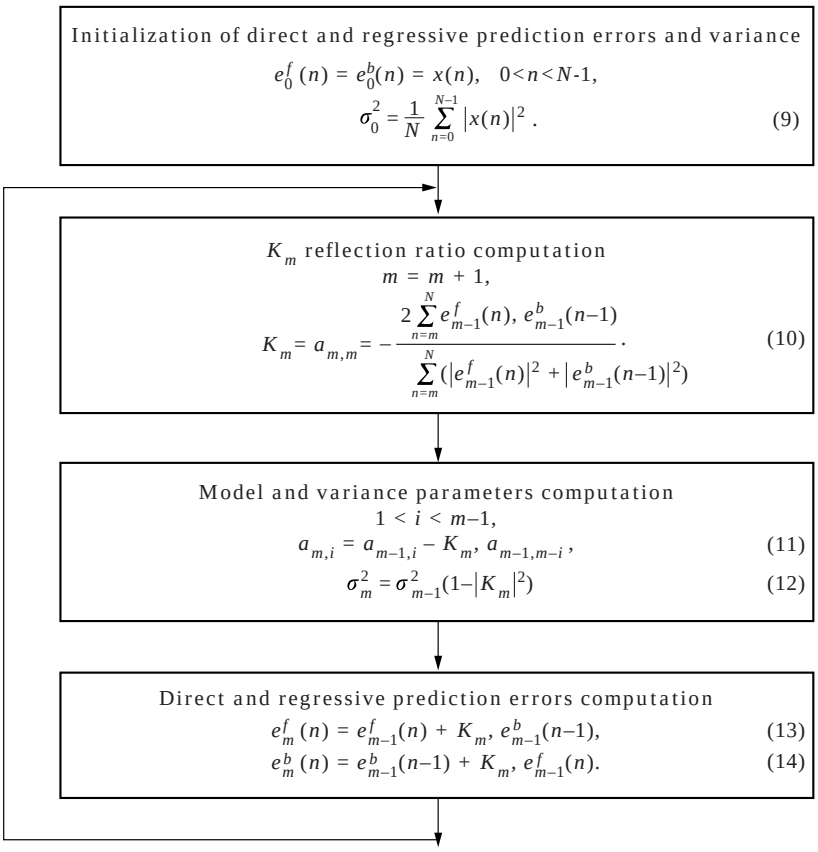

Initialization of direct and regressive prediction errors and variance

$$e_0^f(n) = e_0^b(n) = x(n), \qquad 0 \leqslant n \leqslant N-1,$$

$$\sigma_0^2 = \frac{1}{N}\sum_{n=0}^{N-1} |x(n)|^2. \tag{9}$$

K_m reflection ratio computation

$$m = m + 1$$

$$K_m = a_{m,m} = -\frac{2\sum_{n=m}^{N} e_{m-1}^f(n) e_{m-1}^b(n-1)}{\sum_{n=m}^{N}(|e_{m-1}^f(n)|^2 + |e_{m-1}^b(n-1)|)^2}. \tag{10}$$

Model and variance parameters computation

$$1 \leqslant i \leqslant m-1,$$

$$a_{m,i} = a_{m-1,i} - K_m a_{m-1,m-i}, \tag{11}$$

$$\sigma_m^2 = \sigma_{m-1}^2 (1 - |K_m|^2). \tag{12}$$

Direct and regressive prediction errors computation

$$e_m^f(n) = e_{m-1}^f(n) + K_m e_{m-1}^b(n-1), \tag{13}$$

$$e_m^b(n) = e_{m-1}^b(n-1) + K_m e_{m-1}^f(n). \tag{14}$$

Here N is the number of samples, and m is the recursivity iteration.

Other techniques such as Capon's or the least recurring square method, to mention some of the most conventional ones, were implemented on other rotating machinery.

Thus, the understanding of parameters and model order enables the computation of power spectrum density through the relation

$$P(f) = \frac{1}{|A(f)|^2} = \frac{\sigma_e^2}{\left|1 + \sum_{i=1}^{p} a_i \, \mathrm{e}^{-2j\pi f T_e}\right|^2}, \tag{15}$$

where a_i denotes the AR filter coefficients, σ_e^2 the white noise variance, p the AR model order and T_e sampling time.

Contrary to conventional techniques the power spectrum density recorded via AR methods did not permit a good assessment of typical frequency amplitude. The advantage of this method lies in the early detection of the defects as well as the dissociation of two neighbour typical frequencies, hence, its importance in conditional maintenance.

One must bear in mind that the recording of an AR spectrum, with vibration signal significance, essentially depends on the number of AR model parameters (called model order filter). Actually, if the selected order is too weak, then the spectrum is smoothed and some information is lost, consequently the method is no longer a high resolution one in this case. On the other hand, if the model order is too high, spectrum stripes with no physical meaning appear in the spectrum [8]. This might be misleading and cause a diagnosis error.

Two order selection criteria were retained: the FPE (Final Predictor Error) (16), the AIC (Akaike Information Criterion) (18) and the MDL (Minimum Description Length) (19) criteria (the numbers here are those of the following equations); these criteria, based on prediction error power, were developed by Akaike; the prediction error power monotonously decreases with filter order, whereas assessed variance increases with order; prediction error-based criteria tend towards a compromise between error power and variance:

The FPE criterion is

$$FPE(p) = V_p \frac{N+p+1}{N-p-1}, \tag{16}$$

where

$$V_p = \frac{\sigma_p^2}{r_{xx}(0)} = \prod_{i=1}^{p} (1 - |K_i|^2), \tag{17}$$

in which V_p denotes the variance of the standardized prediction error and N is the number of samples (time data);

the criterion AIC is

$$AIC(p) = N \ln (V_p) + 2p; \tag{18}$$

the MDL criterion (proposed by Rissanen) is

$$MDL(p) = N \ln (V_p) + p \ln (N). \tag{19}$$

The first term of the AIC criterion is proportional to the maximum likelihood of model assessed parameters and the second term is a bias correction one. The FPE criterion is viewed as the sum of the unpredictable part variance of the observation process and a quantity representing AR parameters' assessment inaccuracy. Research has recently been done on the study and the comparison of various AR model order selection criteria [9]. The AIC criterion was retained for our experiment, for it enabled us to assess quite reasonably the number of AR model parameters, whereas the FPE criterion overestimated model order.

The model order will minimize these criteria. Figure 1 denotes the determination of the model order with the AIC criterion for a number of samples and a frequency range considering. This criterion was obtained with a vibratory signal from a forming press.

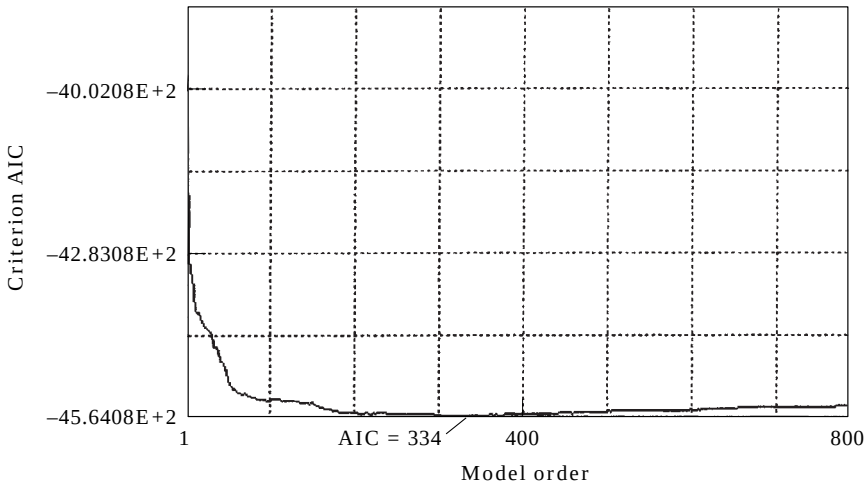

Figure 1. Determination of the model order via the AIC criterion; number of samples 2048, frequency range 100 Hz.

3. EXPERIMENTAL VALIDATION OF AR SPECTRUM ANALYSIS METHODS ON A BENCHTEST

3.1. BENCHTEST AND INSTRUMENTATION SPECIFICATIONS

The monitoring of ball bearing damage was achieved through regular monitoring of 13 ball bearings mounted on a single shaft between the chuck and the tailstock of a horizontal lathe (see Figure 2). The bearings' outer rings were blocked rotationally via a simple assembly (a clamping screw). Furthermore, a small round sticker was stuck on each outer ring perpendicular to the shaft axis so as to facilitate measures.

In these conditions, a single sensor enabled serial monitoring according to a radial direction of the bearing damage. In addition to the accelerometer, the measuring chain incorporated an industrial FFT analyzer with limited characteristics (present frequency range, maximum sample limited to 4096) linked to a microcomputer via an IEEE 448 which enabled the analyzer to be controlled from the computer. The analyzer was only used for time signal acquisition, while the other processing was carried out through a microcomputer and the custom-built piece of software.

Three other sensor positions were chosen (Figure 2 positions 1–3) to study the propagation of the vibrations emitted by mechanical components, on the one hand, and record the various typical frequencies of bearing faults from a single sensor on the other. This enabled the determination of suitable detecting methods according to sensor position.

3.2. THE DIFFERENT TYPES OF FAULTS ON A BALL BEARING

Two types of defects are likely to occur on a ball bearing: defects evenly distributed on the active parts of the bearing, essentially due to bearing manufacture (geometrical defects of elements, defect of surfaces in contact); these defects can only be detected via temporal methods. Such methods use statistical or energy parameters e.g., kurtosis, RMS value, defect factor or other methods

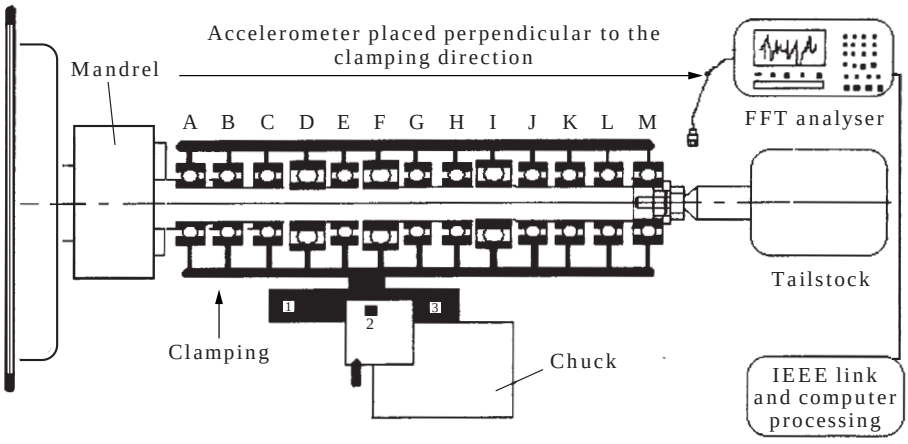

Figure 2. Measuring bench and monitoring device. The 10 6002 SNR bearings are labelled A, B, C, D, E, F, G, H, I, J, K, L, M, and the three 6202EE bearings D, F, I.

in the time domain [1]; defects spotted on elements being part of bearings such as flaking, impression, jamming. Characterized by repetitive shocks, which occur whenever a rolling element encounters the defect, each spotted defect is identified by a recurring frequency which depends on the geometrical characteristics of the bearing and rotational frequency.

If a defect is localized on the outer ring race, a recurring frequency shock f_e appears at each ball pass (20):

$$f_e = \frac{n}{2}\frac{N}{60}\left(1 - \frac{d}{D}\cos\theta\right). \tag{20}$$

Likewise, a defect spotted on the inner ring is characterized by a frequency f_i:

$$f_i = \frac{n}{2}\frac{N}{60}\left(1 + \frac{d}{D}\cos\theta\right). \tag{21}$$

If a defect is spotted on a rolling element, its typical frequency will be

$$f_b = \frac{D}{d}\frac{N}{60}\left(1 - \left(\frac{d}{D}\cos\theta\right)^2\right), \tag{22}$$

where n, N, d, D, θ, respectively denote ball number, shaft rotational speed (rpm), ball diameter, average diameter and contact angle. To spot defects, frequential techniques are the most efficient since they allow both the detection of defects and the monitoring of their propagation.

Bearing specifications are shown in Table 1.

3.3. EXPERIMENTAL RESULTS EXPLOITATION

In this section, defects spotted on bearing moving parts (flaking, strain, imprint) are given particular attention. The clamping, which was achieved via a screw/bolt on the outer ring, allows a punctual load to be applied in a given direction. The generated stress, in turn, engenders fatigue in two given points on the ring. It

TABLE 1

Typical fault frequencies

Bearing specifications	6002 bearing	6202 bearing
Average diameter (mm)	23·5	25
Ball number	9	8
Ball diameter (mm)	4·7	6
Contact angle (°)	945	945
Outer ring speed (rpm)	0	0
Defect localized on the outer ring (Hz)	56·7	47·8
Defect localized on the inner ring (Hz)	85·05	78·12
Defect localized on a rolling element (Hz)	75·6	61·84

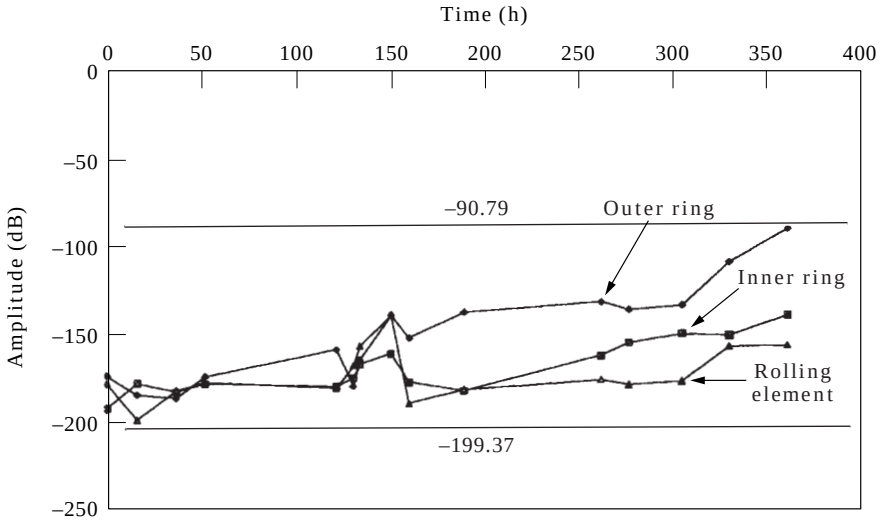

Figure 3. Evolution of the frequency amplitude characteristic of bearing A defects.

causes the appearance of an imprint whose evolution explains the higher vibration level at typical outer-ring-linked-defect frequency (see Figure 3).

3.3.1. *Experimental results analysis on the* 6002 *bearing*

The experiment consisted of monitoring the evolution of the spectrum which is characteristic of each bearing on a time scale, and, in particular, the amplitude of the frequencies which are typical of the localized defects. This evolution is characterized by (i) an increase in the overall level; (ii) the appearance of the harmonics of different typical fault frequencies; and (iii) the appearance of other phenomena like modulation. Figure 3 displays the tendency curves assessed by AR parametric spectrum analysis of the frequencies, which are characteristic of bearing A defects.

Initially both (conventional and parametric) analysis methods give a fault-free spectral signature for each bearing. Despite the similarity of the spectra gained with the two methods, the overall amplitude differs between spectra. Actually, both techniques do not possess the same statistical characteristics. Moreover, for a judiciously selected model (depending on the order selection criterion and the sample number), the AR spectrum reveals all the periodic phenomena contained in the vibratory signal. Thus, only the axle rotational speed ($f_r = 15$–75 Hz) and all of its harmonics ranging from 0 to 100 Hz can appear on each bearing spectrum. The other peaks correspond to lathe kinematic frequencies.

After 200 operating hours, each tendency curve regularly increases, especially the 6002 bearing outer ring defect. The parametric spectrum reveals the typical groove of the fault localized on the outer ring (see Figure 4). As a result, the first signs of damaging of this latter can be assumed. However, even though the peak seems very high at this frequency, nothing can be concluded about the fault seriousness. The corresponding amplitude varies little compared to the previous values as the evolution of the tendency curve shows. As far as monitoring is

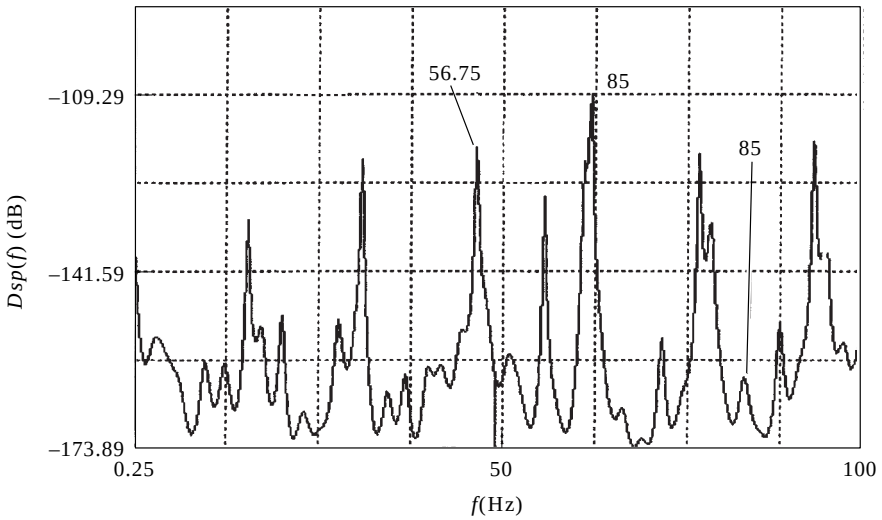

Figure 4. A bearing spectrum after 200 operating hours; Burg (110); appearance of the defect spotted on the outer ring (56·75 Hz).

concerned, it is the amplitude's increasing speed which provides information on the health condition of a component, not the single value at a set time.

On the other hand, the conventional spectrum (correlogram) of bearing A does not display the signs of a defect after 200 operating hours (see Figure 5). This is not a spectrum resolution problem since the selected measuring parameters were computed so as to enable the localization of typical bearing fault stripes. The conventional spectrum does not highlight the low amplitude variations of the typical stripes as far as the whole is concerned. The amplitude of harmonic 3 is much higher than those of typical close frequencies.

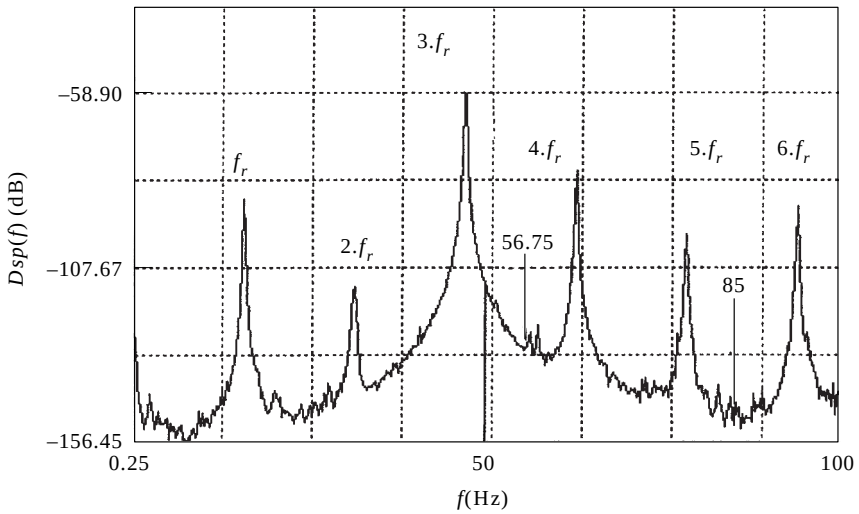

Figure 5. Conventional bearing A (correlogram) after 200 operating hours.

The p order of the AR model steadily increased as time passed. This can be explained by the fact that the number of spectrum stripes increases as the bearing deteriorates. In fact the number of model parameters is strongly linked to the number of periodic signals contained in the vibration signal. The model is determined for a given operating condition at a given time. When the bearing deteriorates, the previous model cannot be adapted to the new condition. Thus, it is redefined anew.

Among the three selection criteria of the selected order, the Akaike (AIC) criterion seems to be the best to assess the parameters number of the AR model. The MDL criterion often underestimates model order, whereas the FPE overestimates it. These order selection criteria do not possess the same statistical properties, and most of the time, the important decrease in the signal-to-noise ratio may result in an overestimation of the AR model order whatever the retained criterion.

That the retained model order does not correspond to the exact model order but is close, does not mean a strong variation at the level of the overall amplitude of the computed spectrum. A close to minimum p value can then be retained via the order selection criterion.

3.3.2. 6202*EE bearings* (D, F, I) *experimental analysis*

The tendency curves of the SNR bearings with 6202EE reference have features which are analogous to the 6002 bearings, as shown in Figure 6.

As in the previous case, at the beginning (conventional or parametric) bearing F spectra display only the output shaft rotational speed (f_r) with its harmonics in the frequency range as well as lathe kinematic frequencies. All of the phenomena previously described with the 6202EE bearings are encountered again. The amplitude of each characteristic fault frequency of 6202EE bearing varies on average (about -160 dB; Figure 6) for the 0–200 operating hour period. It begins

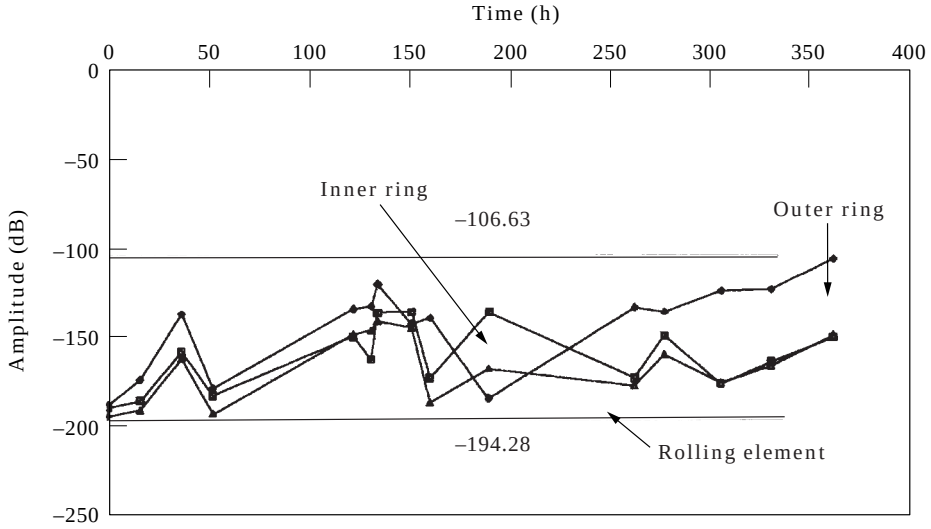

Figure 6. Advancement of typical frequency amplitudes of the bearing F defects.

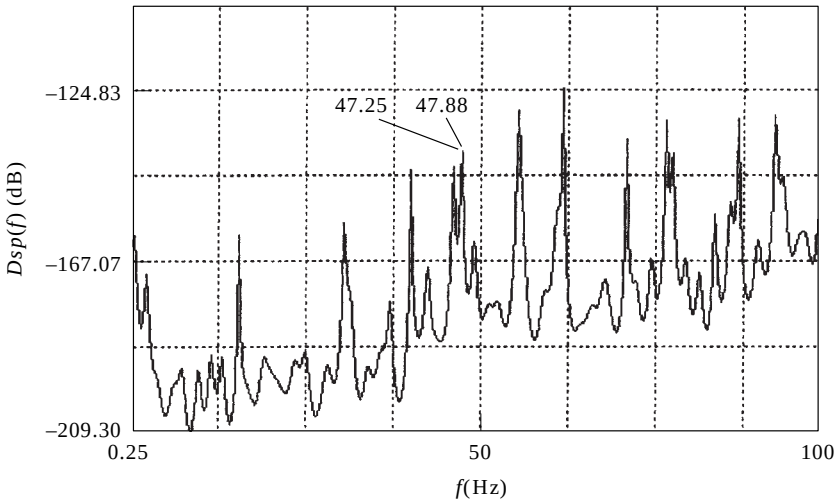

Figure 7. Bearing F parametric spectrum after 350 operating hours. Note appearance of peak at 47·88 Hz due to the outer ring defect.

to increase after 200 h and it is more noticeable with the amplitude of the defect localized on the outer ring (47·88 Hz). The parametric spectrum (see Figure 7) of each reveals the first damaging signs of this component. In contrast, the conventional correlogram-type spectrum (see Figure 8) displays a dynamic problem linked to spectrum stripes width. This problem is even greater for 6202EE bearings since the harmonic 3 of the output shaft rotational speed (47·25 Hz) is very close to the localized defect typical frequency on the outer ring (47·88 Hz). The same applies to the fault spotted on the inner ring at the 78·12 Hz frequency while the harmonic 5 of shaft rotational speed (15·75 Hz) is at 78·75 Hz.

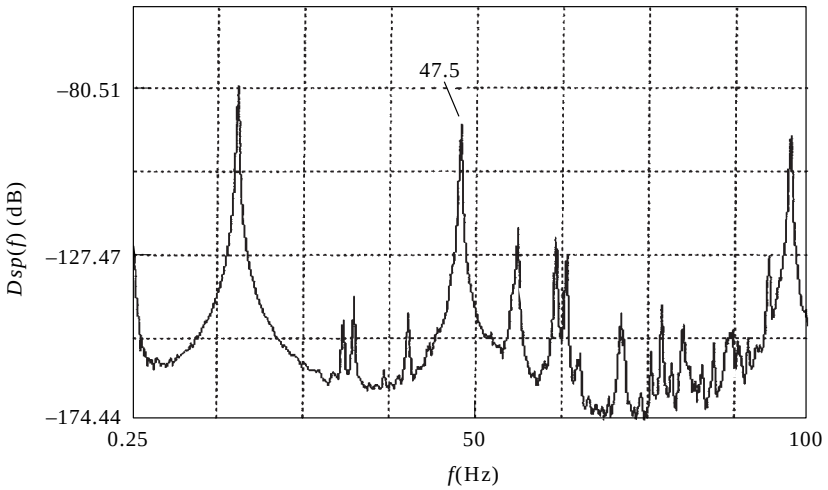

Figure 8. Conventional bearing F spectrum after experimental testing.

In summary, parametric spectral assessment techniques are high-resolution methods and thus enable the detection of the first signs of a fault localized on a mechanical component. Then, they may complement conventional methods based on the Fourier transform which still remain the easiest when the component vibratory signature does not show the frequency characteristics of very close defects that devices cannot dissociate.

3.3.3. *Experimental results from the three sensor positions* (1–3)

The sensor was placed in three different positions (Figure 2: positions 1–3) in such a way as to study the propagation of vibrations emitted by various mechanical components and recover the whole set of typical fault frequencies on different bearing types. This study is essential in so far as (i) each sensitive rotating machinery component is not accessible via a sensor; and (ii) the monitoring chain installation cost by reducing the amount of sensors is required. It is important, too, to point out that time techniques are no longer suitable for bearing damage monitoring since the vibratory signal obtained denotes the vibratory signature of the whole component set. Hence, only frequency analysis enables the detection and the monitoring of the (6002 and 6202EE) bearing damage advancement. Whatever the spectrum assessment in use, the 10 6002 and the three 6202EE bearings display the same frequencies which are typical of localized faults; thus, it is extremely difficult to identify the bearing(s) on which a defect appears. Bearing vibratory signatures have different wavelengths, but, in terms of frequential localization, faults are blurred for each of the types.

The amplitude corresponding to each localized defect typical frequency is the output of the superposition of the 13 bearings' vibratory signatures when these faults are present.

The tendency curves for both types of bearings and the sensor placed in position 1 or 3 evolve as near neighbours in the same way as those obtained when the sensor is placed on each bearing (see Figures 9–12).

The most prominent defects on the outer ring located at 56·75 Hz for the 6002 bearing and at 48 Hz for the 6202EE are present with equivalent respective amplitudes on positions 1 and 3, positions which are symmetrical on the chuck (see Figures 13 and 15 of section 4). Their amplitudes are strongly lowered on the recording in position 2 where the sensor is placed on the chuck that softens vibrations.

The study of the vibration propagation phenomenon in a machine frame is thus preponderant. The understanding of these phenomena allows the determination of ideal sensor positions likely to record a maximum of information in the best conditions. It is actually useless to develop high-resolution spectrum analysis methods if the information is recorded in a position where this information is masked, as shown on position 2 for instance.

To conclude, sensor positioning is essential; however, the detection problem of faults localized on two identical bearings cannot be solved with these methods.

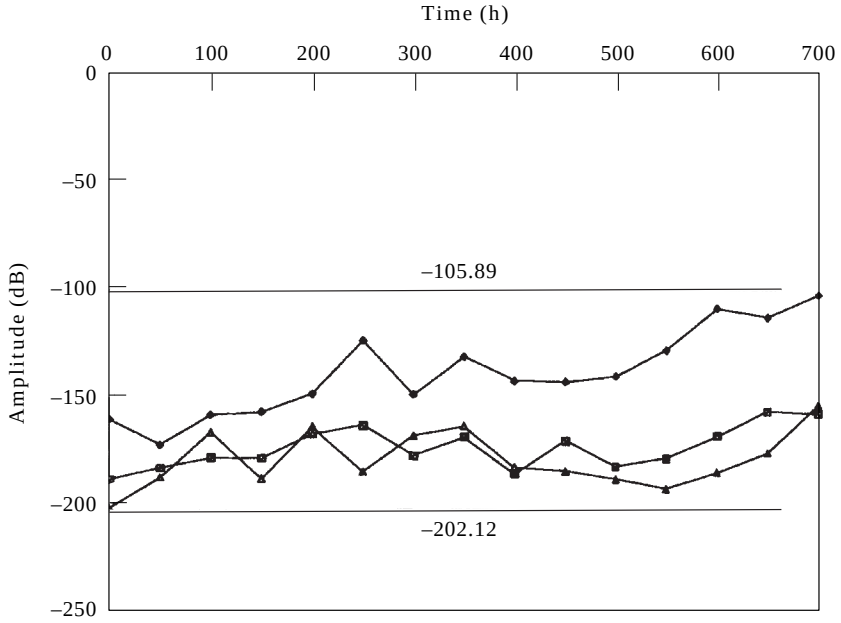

Figure 9. Frequency amplitude evolution typical of bearings for a fault at position 1.

3.4. DISCUSSION

The frequency analysis has shown the benefits of the AR spectrum techniques over conventional ones (correlogram). Burg's algorithm-based parametric spectrum assessment allows early damage detection and fault evolution monitoring of bearings. This can be explained because this technique detects all of the recurring phenomena contained in the vibratory signal. This is a

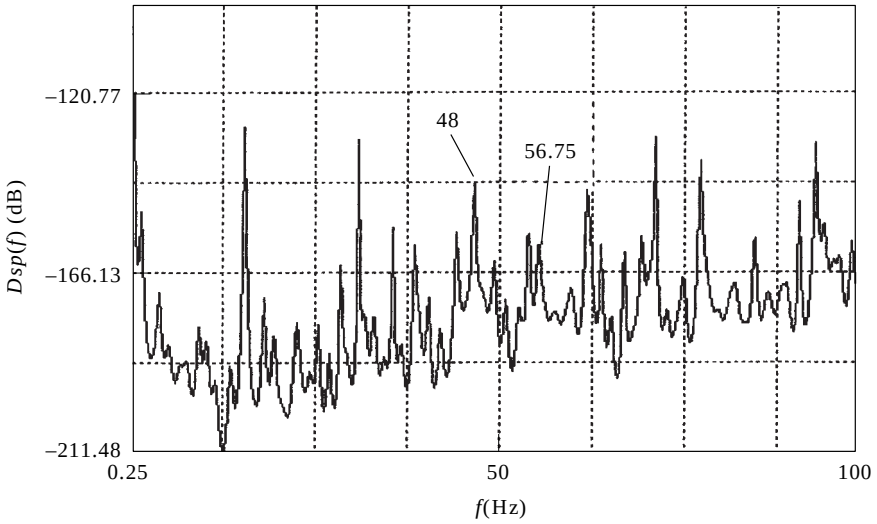

Figure 10. AR spectrum after 150 operating hours. Appearance of the defect localized on the outer ring; sensor placed in position 1.

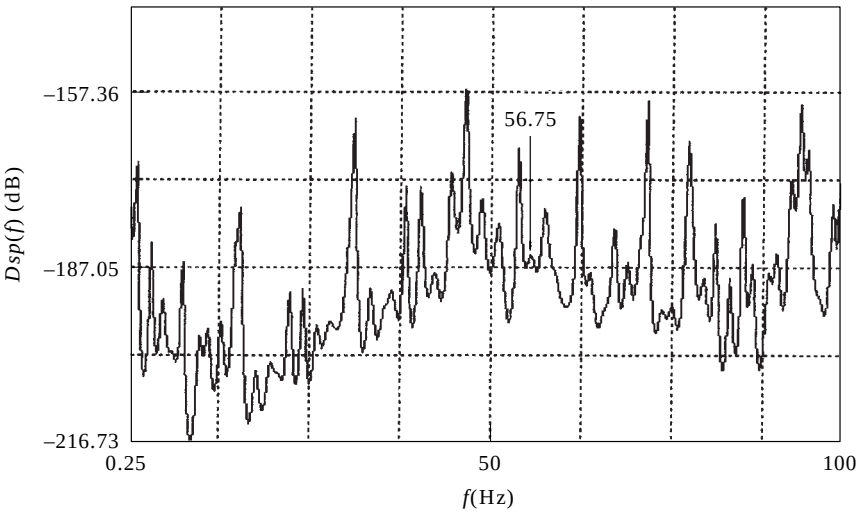

Figure 11. AR spectrum after 150 operating hours. The amplitude of the fault localized on the outer ring is weak; sensor placed in position 2.

high-resolution method which also softens noises. Thus, bearing faults can be detected more quickly.

Model order selection has also been shown to be important. It cannot be over- or underestimated since this might result in significant errors in spectrum computation and completely incorrect interpretations.

Finally, emphasis has been placed on the possible ability of these high-resolution methods to recover the vibratory signature of the complete set of monitored components with a small number of judiciously placed sensors. These complex techniques do not have to replace conventional methods, but complement them.

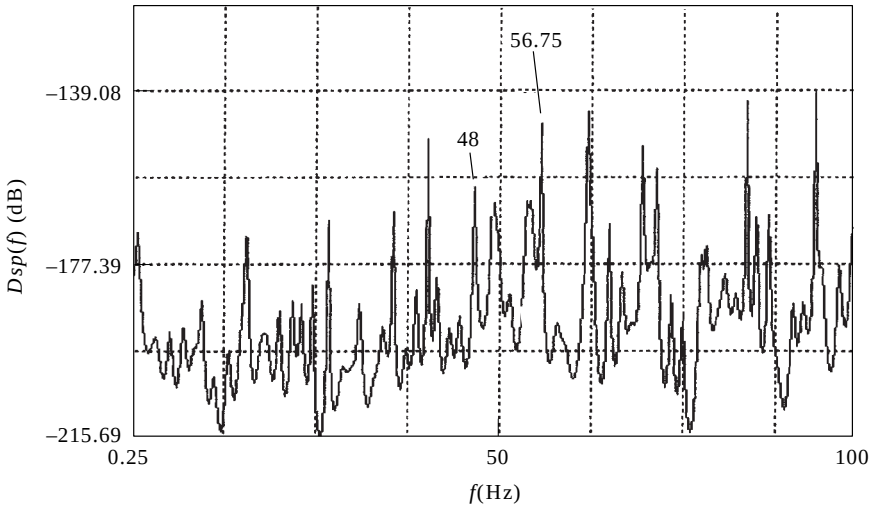

Figure 12. AR spectrum after 150 operating hours. Outer ring localized amplitude; sensor in position 3.

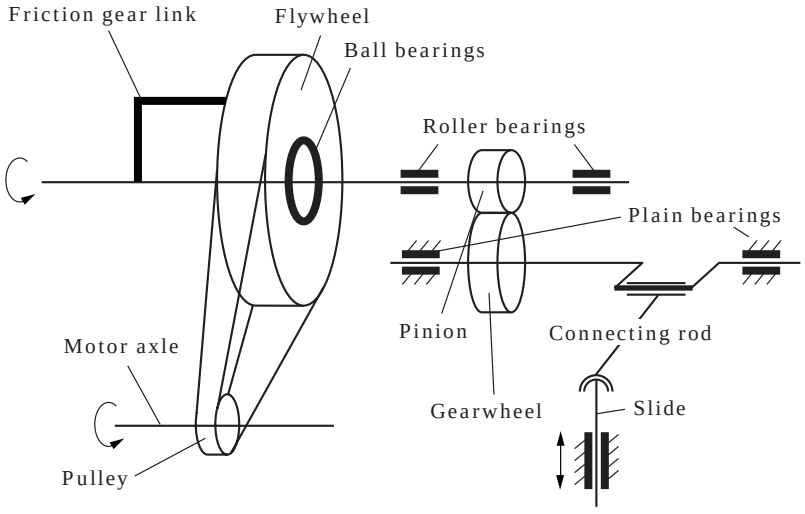

Figure 13. Two-axle press.

Nevertheless, in the case of identical components, the identification of the one which has got a defect cannot be achieved without complementary techniques.

Thus, AR spectrum analysis has been implemented on a device whose unexpected halts result in hefty financial loss: a forming press.

4. PARAMETRIC TECHNIQUES IMPLEMENTATION ON A FORMING PRESS

4.1. FORMING PRESS KINEMATICS STUDY

The study focuses on a swan-neck forming press with a 125-ton capacity (see Figure 13).

The press consists of a frame which drives the shaft through two plain bearings (bronze rings). This shaft acts as a cam in order to convert a rod/strut continuous motion into an alternative rectilinear one. It also drives the flywheel through a belt-based system. The shaft's rotational motion is transmitted via a temporary coupling of the friction gear type. It is slowed down and ground to a half by a friction brake. The press hash two periodic operating modes and an *ad hoc* operating mode. For this study, research was limited to the two periodic modes in which the press behaves like rotating machinery.

4.1.1. *Waiting mode*

In this mode, one gear is not excited; only the flywheel, the driving belt and the motor are operating. The flywheel is mounted freely in rotation on the primary shaft and the brace slide set is insert. In these conditions, only the motor (6), the driving belt (3), the flywheel (8) and the flywheel/primary shaft link ball bearing (9) can monitored (see Figure 14).

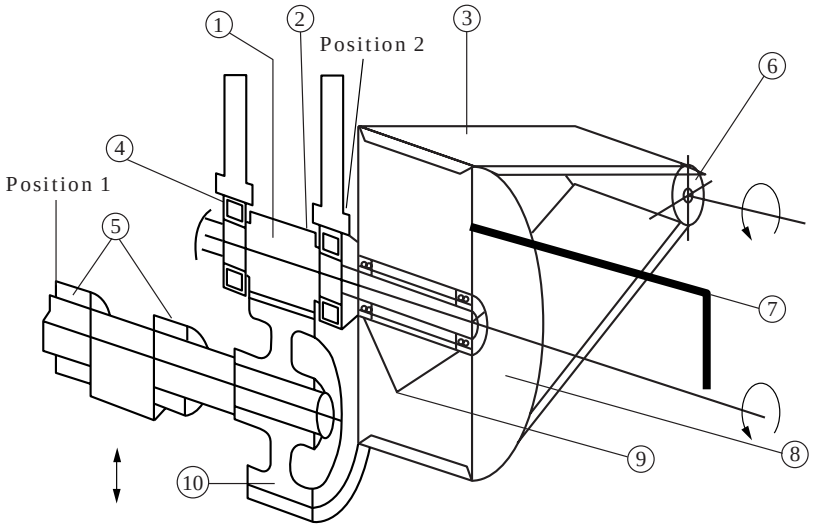

Figure 14. Press driving line.

4.1.2. *Continuous mode*

Here, the gear is excited, and all parts are moving. The press behaves like rotating machinery and the dynamic stress is periodic. The flywheel drives the brace rotationally through the pinions (1) and (10). The brace imposes an up-and-down movement to the slide which contains the forming tool. For this operating mode, motion transmissions (belt, pinion) as well as bearing (fluids (5), rollers (2) and (4)) can be monitored (see Figure 4).

4.2. PROBLEM FORMULATION

The experimental problems encountered were (i) the positions which are to be selected for accelerometers in order to recover as much information as possible; (ii) the optimal motor rotational speed enabling the best localization of typical mechanical parts' faults depending on motor shaft speed; and (iii) the typical device frequencies which can be monitored, and the different fault spectrum indication.

The choice of the accelerometer positions is guided by the accessibility of machine components to be monitored, as well as the propagation of frame vibrations. The restriction linked to component accessibility has led us to consider two positions: close to the flywheel (position 1), which enables the monitoring of components linked to the primary shaft and the flywheel; and close to the slide (position 2), so as to monitor particularly the components linked to the brace (pinion, fluid bearings).

Forming presses are machines with low shaft rotation speeds. The press which was the object of this study had two conical roller bearings having almost identical technical features. Very close typical frequencies resulted from this specificity. Located very close to each other, the monitoring of the two bearings could be achieved only via the same spectrum. With the typical frequencies depending on their size and shaft rotational speeds, the most judicious speed was also the highest.

When the motor rotational speed increased, the interval between two typical component defect frequencies increased, this allowed each typical frequency to be displayed more clearly on the spectrum.

In fact, when the motor rotational speed increases, the interval between two typical components fault frequencies increases too; this allows all the characteristic frequencies to be revealed on the spectrum. However, by increasing motor rotational speed, it is necessary to increase the useful frequency range of the measuring apparatus when acquiring the vibratory signal, which tends to reduce spectrum resolution.

Therefore, compromise between rotational speed and spectrum resolution needs to be determined so as to obtain good vibration measurement efficiency. Therefore, ideal press rotational speed must be determined along with the most appropriate spectrum analyzer settings during signal acquisition.

Typical fault frequencies and exciting source analysis according to motor rotational speed enables the following to be specified: (i) the sample number to take; (ii) the frequency range of the analysis; (iii) the motor rotational speed in order to obtain optimal spectrum resolution.

When the press is in standby mode the typical frequencies that can be monitored correspond either to motor shaft and flywheel unbalances, to belt motion driving, or to flywheel/primary shaft link rolling bearings. For an 80-rpm motor shaft rotational speed, typical fault frequencies are reported in Table 2.

4.3. RESULTS EXPLOITATION

Given the number of mechanical components to be monitored on the press, the recorded vibration signal spectrum is very rich. Moreover, each typical fault frequency generates harmonics whose number depends essentially on the nature and seriousness of the localized defect. However, these harmonics cannot be interpreted to characterize a component defect since the appearance and disappearance of some harmonics are still randomly generated and depend on several factors (rational speed variation, external parasites, . . .). Only amplitude evolution monitoring corresponding to the characteristic fault frequency remains efficient when characterizing component faults. To stress the contribution of ARR

TABLE 2

Components to be monitored in position 1*—waiting mode*

Component	Typical frequencies defect	Output shaft speed (Hz)	(rpm)	Number of samples	Frequency range	Sensor position
Motor shaft	Unbalance	45·07	80	1024	50	1
Flywheel	Unbalance	7·12	80	1024	50	1
Belt	Driving	5·20	80	1024	50	1
Bearing 6220	Inner ring defect	42·04	80	1024	50	1
Bearing 6220	Outer ring defect	29·13	80	1024	50	1
Bearing 6220	Roller element defect	37·93	80	1024	50	1

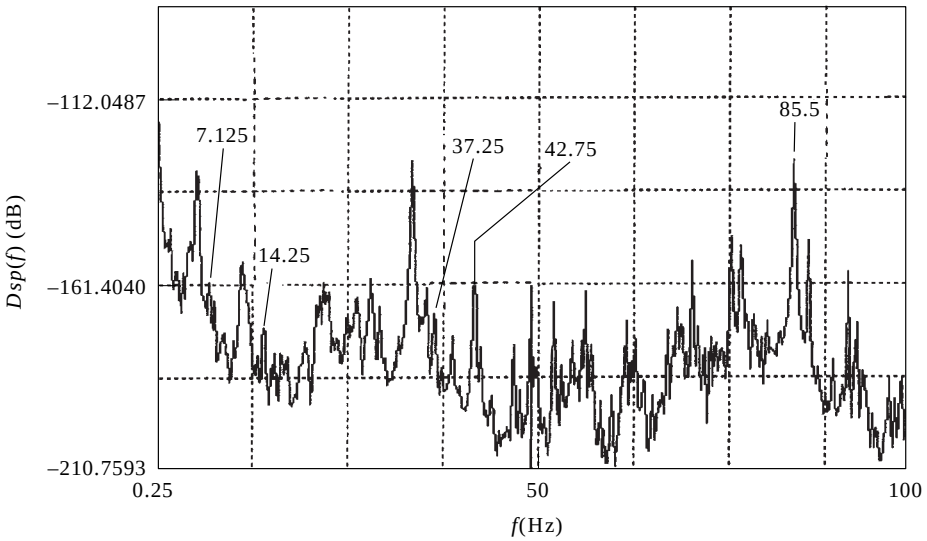

Figure 15. Conventional spectrum (correlogram).

parametric methods three recordings are presented which display the evolution of various faults localized on press components. These three recordings correspond to the waiting mode, where the sensor is placed in position 1. Theoretically, in these conditions, six typical fault frequencies should be detected if the components to be monitored are damaged or on the verge of sustaining damage (see Table 2).

4.3.1. *Recording* 1

From the first recording, the major difference between the two (conventional and parametric) techniques have been highlighted at the localization level of typical component defects. Flywheel unbalance (7·12 Hz) is detected in the conventional spectrum (see Figure 15) with an amplitude of 158·54 dB. This frequency generated three frequencies on the spectrum.

Theoretically, the typical frequency of 6202EE ball bearing defects is around 37·93 Hz. The 37·25-Hz peak on the spectrum could then be considered as a ball bearing defect but the next measure would have to be awaited to ensure the exact position of the rolling element fault frequency. Note that the 100-Hz range has been preferred to the 50-Hz range. To offset this difference, 2048 samples were taken of 1024. The presence of other peaks which are not harmonics or modulations is ignored.

In the AR spectrum (see Figure 16), on the other hand, the presence of flywheel unbalance at 7·12 Hz and the motor shaft rotational speed at 45·07 Hz that cannot be detected on the conventional spectrum can be seen. The presence of two frequency harmonics [harmonic 1: 11·75 Hz ($-126{\cdot}2$ dB) and harmonic 2: 22·5 Hz ($-122{\cdot}43$ dB)] shows a belt-driving fault.

No peak on typical 6202EE bearings fault frequencies is detected, which indicates that there is no damage.

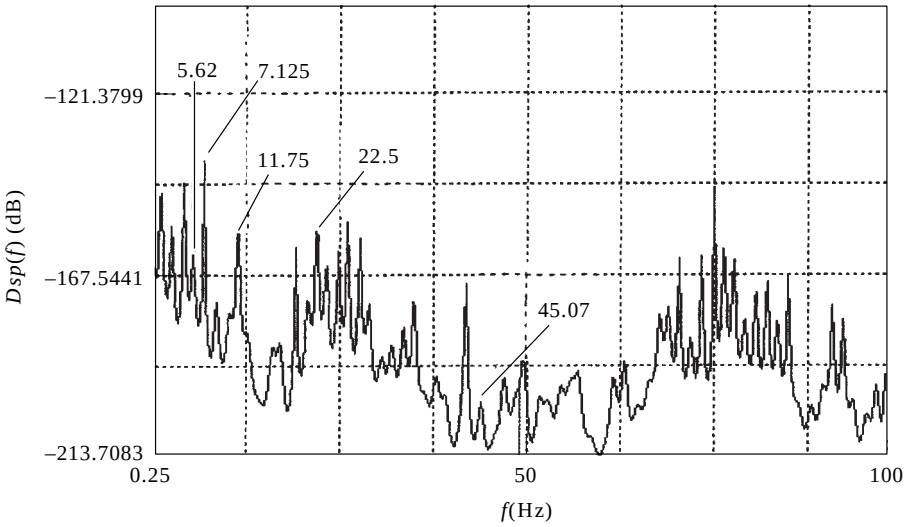

Figure 16. Parametric order (p order = 170 via the AIC criterion).

However, it is worth noticing that Burg's algorithm is sensitive to noise effects and that model order selection plays an important part in revealing all of the recurring phenomena. This is one of the major problems related to signal parametric modelling.

4.3.2. *Recording* 2

The results obtained confirm the previous results. As for recording 1, flywheel unbalance amplitude has increased and belt-driving fault has appeared at 5·62 Hz (see Figure 17). Motor shaft unbalance does not appear on the conventional spectrum. There is no significant peak of the 6202EE bearing condition. All this indicates that it is still in perfect working order.

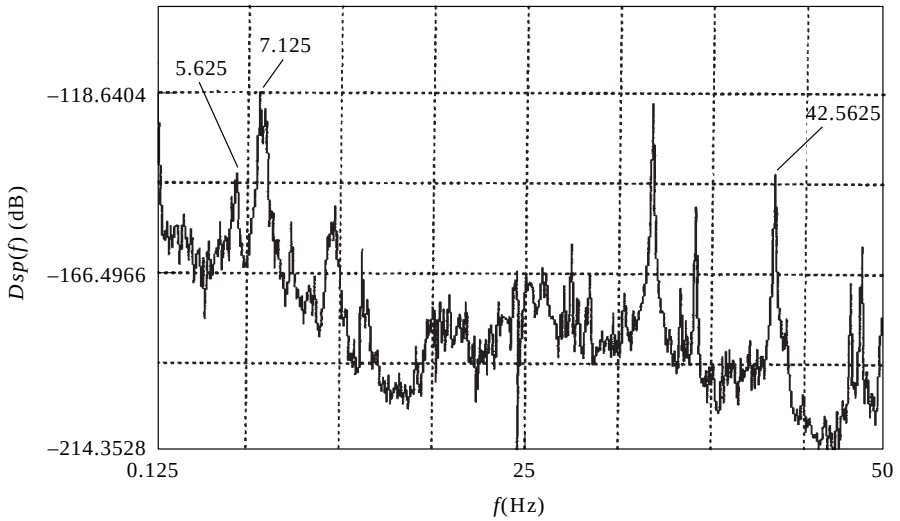

Figure 17. Conventional spectrum (correlogram).

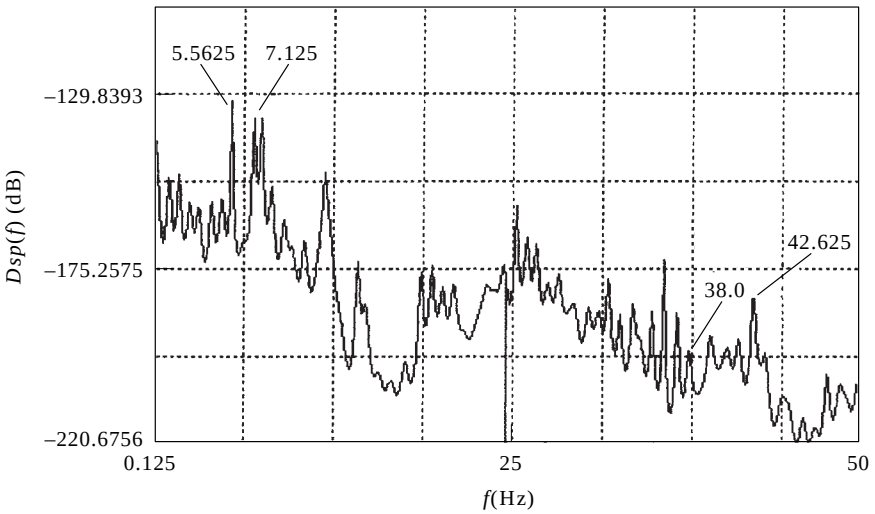

Figure 18. Parametric order (p order via the AIC criterion).

However, in the parametric spectrum (see Figure 18), a 6202EE roller bearing element fault begins to appear and is characterized by a 38-Hz peak. This confirms the usefulness of parametric techniques in early fault detection, but the same previous phenomena are still encountered.

4.3.3. *Recording* 3

Compared with the previous recordings in the same mode, the 6202EE bearing outer ring defect appears at 29·06 Hz (−165·98 dB; see Figure 19). Motor shaft unbalance appears at 44·87 Hz with an amplitude of −195·83 dB. Flywheel unbalance, which is around 7·12 Hz with an amplitude of −172·46 dB, generates five harmonics. Likewise, the belt driving defect appears at 5·12 Hz with an

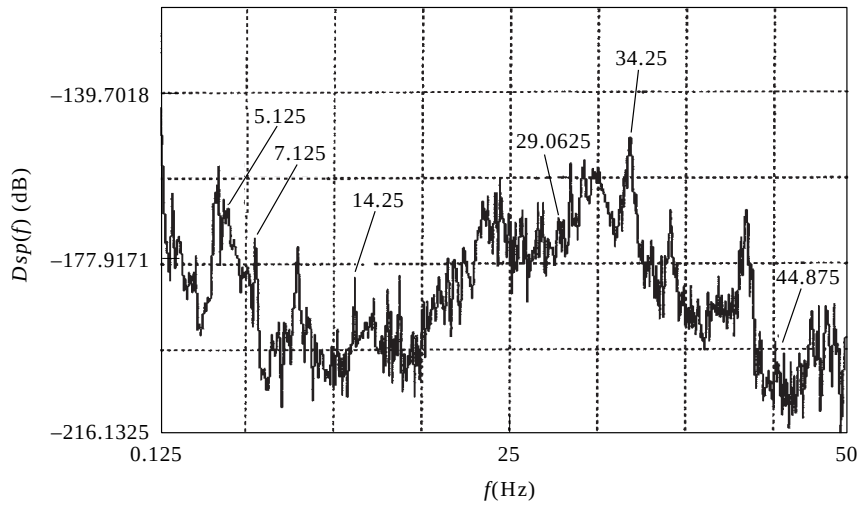

Figure 19. Conventional spectrum (correlogram).

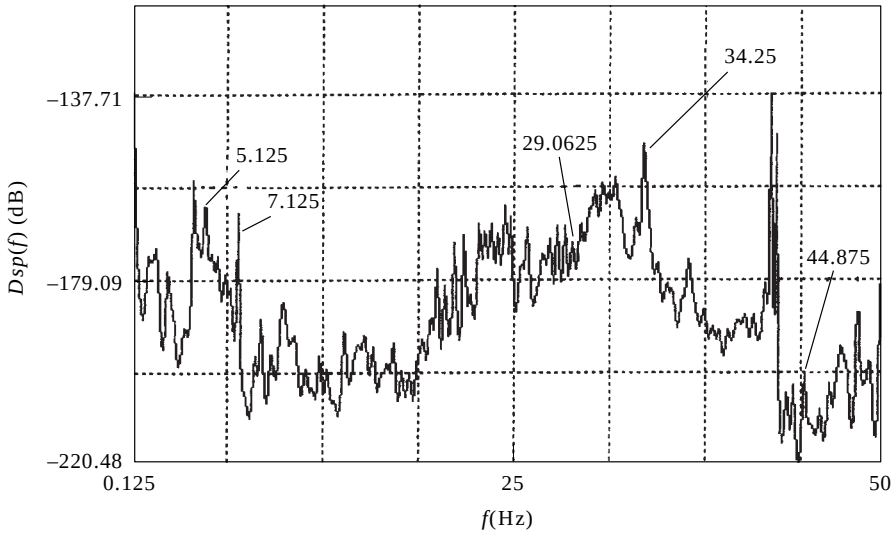

Figure 20. Parametric spectrum.

amplitude of −166·80 dB. This frequency, typical of the belt driving, generates harmonics 2, 4 and 5, while harmonic 3 is absent. As before, these are not reliable in determining the severity of the fault.

The parametric spectrum (see Figure 20) confirms the appearance of the outer ring defect (29·06 Hz). The other previously detected faults are also present on this spectrum.

4.4. DISCUSSION

Throughout this experiment, the number of faults increases, and in some cases these defects are visible only on the parametric spectrum at an early stage. This is because for a given measure of parameters setting (sample number, frequency range, signal-to-noise ratio) parametric spectrum analysis techniques do offer a better resolution than conventional Fourier transform-based methods. As pointed

TABLE 3

Summary

	Conventional spectrum			Parametric spectrum		
Localized defects	Recording 1	Recording 2	Recording 3	Recording 1	Recording 2	Recording 3
Flywheel unbalance	Yes	Yes	Yes	Yes	Yes	Yes
Driving defect	No	Yes	Yes	Yes	Yes	Yes
Motor shaft unbalance	No	No	Yes	Yes	Yes	Yes
Ball defect	No	No	No	No	Yes	Yes
Outer ring defect	No	No	Yes	No	No	Yes
Inner ring defect	No	No	No	No	No	No

out at the beginning of the recordings, these so-called high-resolution techniques must be implemented very cautiously due to the computational complexity. These methods should not replace conventional spectrum analysis techniques but complement them when a large spectrum resolution is required, to dissociate neighbour typical grooves, or when the vibratory signature of the entire system has to be achieved when individual components cannot be monitored. Table 3 illustrates the various typical fault frequencies observed throughout the measuring campaign for each implemented method and for a standby operating mode.

5. CONCLUSION

The problems related to press kinematics do not allow the use of all signal processing digital methods. Hence, spectrum analysis remains the most efficient tool to localize and monitor the damping condition of various components on an industrial site.

This study has established that parametric techniques along with conventional methods bring extra information since they display all of the signals occurring in a vibratory signature. This enables the detection of a fault at an early stage and the monitoring of its evolution on a time scale. Therefore, it is a worthwhile technique at the conditional method level.

For machine accessibility purposes, the measuring campaign was limited to nine months. This time period is not long enough to detect the evolution of the typical frequency amplitudes of identified faults on the machine.

The press has been operating for more than 20 years and the damaging processes of its part are slow; this research warns about the components which are becoming damaged and those which are still in working order. Our research is currently directed towards use of the appropriate vibration signal model like the ARMA model which could permit the correlation between model parameters and typical frequencies contained in the signal. In this case, model parameter evolution monitoring may turn out to be significant for rotating machinery monitoring.

REFERENCES

1. C. Pachaud and C. Fray 1997 *Mécanique Industrielle et Matériaux* **50**(2). Contribution du facteur de crête et du kurtosis l l'identification des défauts induisant des forces impulsionnelles périodiques.
2. D. C. Baillie and J. Mathiew 1996 *Mechanical Systems and Signal Processing* **2,** 1–17. A comparison of autoregressive modelling techniques for fault diagnosis of rolling element bearings.
3. M. K. Stevens and S. L. Marple, Jr. 1981 *Proceedings of the IEEE* **69**, 81–87. Spectrum analysis—a modern perspective.
4. C. Mechefske and J. Mathiew 1992 *Mechanical Systems and Signal Processing* **4**, 297–3077. Fault detection and diagnosis in low speed rolling element bearings part I: the use of parametric spectra.
5. H. Akaike 1974 *Proceedings of the IEEE* **19**, 716–723. A new look at the statistical model identification.
6. S. M. Kay and S. L. Marple 1981 *Proceedings of the IEEE* **69**(11), 81–87. Spectrum analysis—a modern perspective.

7. K. Drouiche, M. Sidahmed and Y. Grenier 1991 *Trailement du signal* **8**(5), 331–343. Détection de défauts d'engrenages par analyse vibratoire.
8. T. Robert and C. Mailhes 1994 *Journal de physique IV* **4**, C5-1383–C5-1386 colloque C5. Effet de perturbation sur l'estimation des modèles autoregressifs.
9. J. R. Dickie and K. Nandi 1994 *Signal Processing* **40**, 239–255. A comparative study of AR order selection methods.